# Quasifree scattering in the preequilibrium region

R. D. Smith and M. Bozoian
*Los Alamos National Laboratory, Los Alamos, New Mexico 87545*
(Received 28 November 1988)

A model for inclusive proton-nucleus scattering which covers the preequilibrium region is developed based on (1) single-step quasifree scattering and (2) the exciton model, which describes emission from 3p2h and higher configurations. Results are compared to data for various nuclei at incident energies from 60 to 200 MeV. The systematics of angle-dependent energy spectra are well reproduced by the model, except in the large-energy-loss region at very forward angles. We find the single-step quasifree scattering constitutes 60% to 80% of the reaction cross section in medium-heavy nuclei, and about 50% in heavy nuclei. The preequilibrium region is therefore dominated by direct single-step reactions.

## I. INTRODUCTION

A variety of theoretical models for precompound or preequilibrium reactions have been developed over the last twenty years, such as the intranuclear cascade model (INC), the "quantum mechanical" model of multistep direct reactions (MSDR), and models based on statistical emission such as the exciton and hybrid models (for a review see Ref. 1). All of these models are based on the idea that the dominant reaction mechanism responsible for preequilibrium spectra in a sequence of nucleon-nucleon collisions leading to particle emission before the energy is dissipated and a compound nucleus is formed. However, they all require phenomenological input in order to give reasonable descriptions of the data. The statistical models are designed primarily to calculate angle-integrated cross sections $d\sigma/d\varepsilon$, and these must be generalized using phenomenological angle- and energy-dependent factors in order to describe double differential cross sections $d^2\sigma/d\Omega\, d\varepsilon$. The MSDR model can describe angular dependence, but it is also phenomenological, since the strength of the effective interaction in the transition matrix elements is adjusted to fit data.

The aim of this paper is to develop a simple model which can describe the angle and energy dependence of preequilibrium spectra without resorting to phenomenology. Our approach is motivated by the fact that in all theoretical models, the largest component of the preequilibrium cross section is due to emission from the first stage of the reaction (i.e., the 2p1h configuration), which we describe in terms of single-step quasifree nucleon-nucleon scattering. In this sense our model is very similar to the work of Chiang and Hüfner,[2] who showed that single-step quasifree scattering dominates the inclusive nucleon-nucleus cross section at energies between 15 and 100 MeV. In their model the preequilibrium cross section was composed of single and double quasifree nucleon-nucleon scattering, and higher-order processes were assumed to lead to compound nucleus formation. We agree with this procedure, but in our model we improve the calculation of the single scattering term with a more accurate treatment of the distortion and the nucleon-nucleon (NN) amplitudes. We will not directly evaluate the double scattering term as they did, because we feel that the approximations they were forced to make, particularly in the evaluation of the distortion, are not adequate at the large scattering angles and relatively low incident energies we are interested in. While a more sophisticated treatment of the double scattering term is possible within the framework of our model, it is numerically very complicated. Instead, we will use the exciton model to describe multistep processes. The great advantage of the exciton model is that it involves relatively simple numerical calculations. As will be discussed below, the exciton (or hybrid) model cannot be consistently applied to the first stage of the reaction, since it assumes all 2p1h states are occupied with equal probability. Nevertheless, it should provide a reasonable description of the multistep processes, where the total energy is shared among many particles and holes, resulting in cross sections which vary slowly with angle and energy transfer. Finally, since we are primarily interested in the preequilibrium contribution to particle emission spectra, we will not include the evaporation spectrum from compound nucleus decay, although it can easily be added to our results.

Section II of this paper briefly describes the exciton model. We use a stripped-down version of the model which removes as much phenomenology as possible. Section III discusses details of the single-step quasifree scattering calculation, which is based on the distorted-wave continuum response model of Ref. 3. This model allows for absorption and momentum transfer in the distortion and uses the NN amplitudes evaluated in the "optimal" frame of Gurvitz.[4] The angle and energy dependence of the final-state absorption is also included in the calculation of the distortion factor $N_{\text{eff}}$. In Sec. IV we describe how to combine the single-step quasifree scattering with the exciton model, and in Sec. V we discuss the results of calculations for a variety of nuclei in the 60–200-MeV energy range.

## II. THE EXCITON MODEL

The preequilibrium spectrum spans the region between very high emission energies, which is dominated by direct

 

reactions, and very low emission energies, which is dominated by isotropic compound-nucleus decay. As such, it shares features of both types of reactions, and is characterized by smooth, forward-peaked angular distributions and high energy emission tails. This, combined with the fact that the nuclear level densities are very high, suggests that a statistical treatment may be adequate.

The exciton model is a semiclassical, statistical description of preequilibrium reactions in which all possible ways of sharing energy between different particle-hole configurations of the same exciton number $n$ (the total number of particles plus holes) are considered equally likely. The mean lifetime of a given exciton state is determined from a time-dependent master equation in which single-particle emission rates compete with the rates for internal transitions which can change the exciton number by $\pm 2$ or 0. In its simplest form, the model describes a cascade beginning with 2p1h states which may either decay by emitting one particle or proceed through binary collisions to the next stage or "generation" which has an extra p-h pair. At each successive generation, the competing rates for cascade versus emission are again calculated. Following the notation of Ref. 5, the double-differential cross section for an incident nucleon of kinetic energy $E$ is given by

$$\frac{d^2\sigma}{d\Omega\, d\varepsilon}=\sigma_R \sum_n \frac{D_n Q(n,\Omega)}{\Lambda_+^{(n)}+\Lambda_c^{(n)}}\rho_n(E,\varepsilon)\lambda_c(\varepsilon) , \tag{1}$$

where $\varepsilon$ is the kinetic energy of the emitted nucleon, and the summation is over successive generations: $n=2$p1h, 3p2h, etc. $\sigma_R$ is the formation cross section which we identify with the total reaction cross section, because at the energy transfers under consideration we neglect the contribution from all reaction mechanisms other than nucleon emission from particle-hole configurations. $\lambda_c(\varepsilon)$ is the single-particle emission rate, and $\rho_n(E,\varepsilon)$ is the probability of finding a particle with energy $\varepsilon$ in an $n$-exciton configuration of total energy $E$, which will be evaluated using a modified version of the Williams level-density formula[6] which takes into account the finite depth of the nuclear potential well. Thus the product $\rho_n(E,\varepsilon)\lambda_c(\varepsilon)$ [which in standard exciton notation is called $W_\nu(n,\varepsilon)$] is the total emission rate per unit energy. $D_n$ is the "depletion factor" which is the probability of making it to the $n$th generation before emitting a particle (see Sec. IV). The combination $D_n Q(n,\Omega)/(\Lambda_+^{(n)}+\Lambda_c^{(n)})$, usually called $\tau(n,\Omega)$, is the mean lifetime of the state $n$ which decays by emitting a particle into the direction $\Omega$.

$\tau(n,\Omega)$ is obtained directly from an angle-dependent master equation which incorporates a free scattering kernel proportional to the NN cross section in the laboratory frame. In the case of isotropic NN scattering, $Q(n,\Omega)$ can be expressed exactly as a sum over the Legendre polynomials $P_l(\cos\theta)$ times the corresponding eigenvalues of the free scattering kernel in the $P_l$ basis.[7] The coefficients of the Legendre polynomials can be adjusted to fit the data, but we will use the exact expression for the isotropic case in order to avoid fitting parameters. The validity of this procedure for calculating angular distributions will be discussed in the last section.

The denominator in Eq. (1) is the sum of integrated emission and intranuclear transition rates given, respectively, by

$$\Lambda_c^{(n)}=\int_0^E d\varepsilon\,\rho_n(E,\varepsilon)\lambda_c(\varepsilon) ,$$
$$\Lambda_+^{(n)}=\int_0^E d\varepsilon\,\rho_n(E,\varepsilon)\lambda_+(\varepsilon) , \tag{2}$$

where $\lambda_+$ is the single-particle intranuclear transition rate. The single-particle rates are given by

$$\lambda_+(\varepsilon)=\frac{v}{\lambda_m},\quad \lambda_m=\frac{m}{m_k}[\bar{\sigma}_{\rm NN}(\varepsilon)\rho_0]^{-1} ,$$
$$\lambda_c(\varepsilon)=\frac{2s_\nu+1}{\pi^2\hbar^3}m\varepsilon\left[1+\frac{\varepsilon}{2m}\right]\sigma_\nu(\varepsilon)Q_\nu(n) . \tag{3}$$

In the first equation $v$ is the velocity, $\lambda_m$ is the mean free path determined from the in-medium NN cross section discussed in the next section, $\rho_0=0.16$ fm$^{-3}$ is the nuclear matter density, and $m_k$ is the nucleon effective mass which accounts for the nonlocality of the optical potential[8] (we take $m_k/m=0.7$). In the second equation, $s_\nu$ and $\sigma_\nu$ are the spin and inverse cross section for an emitted particle of type $\nu$, and the quantity in parentheses is a correction for the relativistic energy. $Q_\nu(n)$ is the fraction of particles of type $\nu$ in the $n$-exciton state. It is approximately determined, as in Ref. 9, from the ratio of $p$-$n$ to $p$-$p$ cross sections and the number of target neutrons ($N$) and protons ($Z$). For incident protons

$$Q_{\rm proton}=\frac{1}{n'}\left[\frac{3N+2Z}{6N+2Z}+\frac{n'-1}{2}\right] ,$$
$$Q_{\rm neutron}=1-Q_{\rm proton} , \tag{4}$$

where $n'$ is the generation number, related to the exciton number by $n=2n'+1$.

## III. QUASIFREE SCATTERING (QFS)

The assumption of statistical emission should only be valid in the later stages of the intranuclear cascade, and it is certainly not valid after only one collision. Therefore, the exciton model should not be applied to the first stage, especially since it assumes complete configuration mixing[5] among all possible 2p1h states of a given energy, so that each state is populated with equal probability, weighted by the level density. Immediately after the first collision there is only one 2p1h state excited. And while the residual p-h interaction can mix this with other 2p1h states of the same energy, this has a relatively weak effect on the single-step scattering, and it clearly does not lead to equal population of all energetically available states. Instead, the probability of exciting a given 2p1h state is determined by the energy and angle dependence of nucleon-nucleon scattering in the medium. We will therefore describe the first stage in terms of direct, quasifree NN scattering.

The models of quasifree scattering which we will use are described in detail in Ref. 3. A simple version of the single-step $N$-nucleus cross section, which includes most

of the essential physics, is given by

$$\frac{d^2\sigma}{d\Omega\, d\varepsilon} = N_{\rm eff}(\theta,\omega) C |f_{\rm opt}(q,\omega)|^2 R(q,\omega) , \quad (5)$$

where $q$ and $\omega$ are the momentum and energy transfer, and $\theta$ is the laboratory scattering angle. $f_{\rm opt}$ is the NN amplitude evaluated in the "optimal" frame, and $C$ is a kinematic factor[3] which approaches $4k'/k$ in the nonrelativistic limit. $R(q,\omega)$ is the nuclear response function which will be calculated in a Fermi-gas model, and $N_{\rm eff}$ is an angle- and energy-dependent normalization which accounts for attenuation in the initial and final states due to the strong absorption of the probe. In the next three subsections we will discuss specifically how these quantities are evaluated.

### A. Initial- and final-state absorption

In Glauber theory, $N_{\rm eff}$ is calculated by assuming the projectile traverses an essentially straight-line path through the nucleus. Since we will be dealing with large-angle scattering, this is not an adequate approximation. Instead, we calculate $N_{\rm eff}$ assuming straight-line propogation only in the initial and final states and allow the projectile to change direction on the hard collision as dictated by the scattering angle. Furthermore, the total NN cross section is evaluated in the final state at the lower energy $E-\omega$. Thus $N_{\rm eff}$ is given by

$$N_{\rm eff}(\theta,\omega) = \int d^3r \exp\left[-\sigma \int_{-\infty}^{r} dr' \rho(r')\right] \rho(r) \times \exp\left[-\sigma'(\omega) \int_{r}^{\infty'(\theta)} dr' \rho(r')\right] , \quad (6)$$

where $\sigma = \bar{\sigma}_{\rm NN}(E)$, $\sigma'(\omega) = \bar{\sigma}_{\rm NN}(E-\omega)$, and $\bar{\sigma}_{\rm NN}$ is the in-medium total NN cross section. Figure 1 illustrates a typical path through the nucleus taken by the projectile, which has a hard collision at the point $\mathbf{r}$. Integrals over $r'$ of the nuclear density in Eq. (6) are along these paths. The in-medium NN cross section is determined, as in Refs. 3 and 10, from the volume integral of the phenomenological imaginary optical potential:

$$\bar{\sigma}_{\rm NN}(E) = \frac{2m}{\hbar k} \int d^3r [W(r,E)/A] = \frac{2m}{\hbar k} J_W/A , \quad (7)$$

which is exact in the limit of a zero-range NN interaction. Values of $J_W/A$ have been obtained in the energy region $40 < E < 1000$ MeV from optical-model analysis of elastic scattering data.[11] We adopt the following parametrization of these results:

$$J_W/A = 100 \frac{E^2}{E^2+18^2} \text{ MeV fm}^3 \quad (E < 164 \text{ MeV}) = 0.6E \text{ MeV fm}^3 \quad (E > 164 \text{ MeV}) . \quad (8)$$

The low-energy behavior is the same as the parametrization of the single-particle imaginary self-energy used in Ref. 12. Figure 2 shows $\bar{\sigma}_{\rm NN}(E)$ calculated from Eqs. (7) and (8). For comparison, the free (isospin-averaged) NN cross section determined from the Arndt phase shift solutions[13] is shown by the dashed line. Due to Pauli blocking, the in-medium cross section must vanish at the Fermi energy ($E=0$), but it has a pronounced peak near 40 MeV, reflecting the rise in the free NN cross section at low energy.

Equation (6) agrees with the standard Glauber theory formula only at $\theta=0$ and $\omega=0$. At back angles $N_{\rm eff}$ is typically $\sim 40\%$ larger than at forward angles. It can also vary substantially with $\omega$ due to the energy dependence of $\bar{\sigma}_{\rm NN}$.

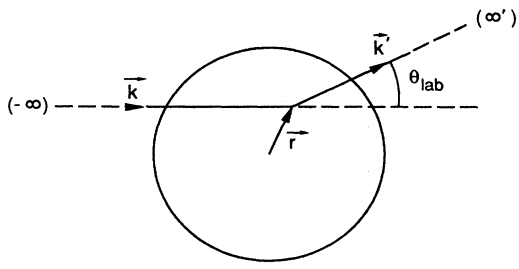


FIG. 1. Typical path through the nucleus taken by the projectile, which has a hard collision at the point r. Integrals of the density times the NN cross section in Eq. (6) are along this path.

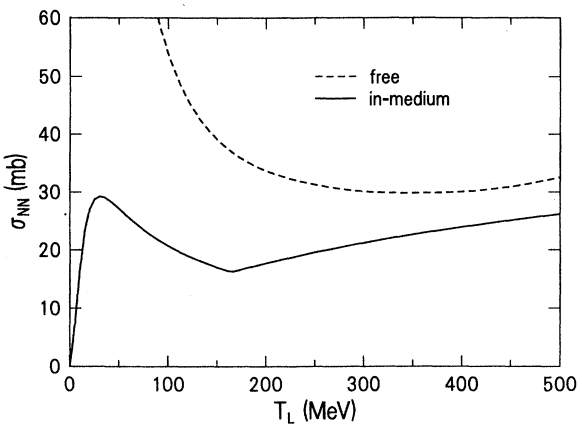


FIG. 2. The in-medium NN total cross section (solid line) based on Eqs. (7) and (8), plotted versus the laboratory kinetic energy $T_L$. Dashed lines show the free (isospin-averaged) NN cross section.

### B. NN amplitudes

We now turn to the question of how to evaluate the two-body amplitudes which describe a quasielastic collision. In the impulse approximation they are associated with the free NN amplitudes derived from experimental phase shifts. These depend not only on the incident energy and momentum transfer, but also on the momentum of the struck nucleon, which varies due to its Fermi motion. In order to calculate quasielastic cross sections it is in principle necessary to integrate over the struck nucleon's momentum. This problem is greatly simplified if the two-body amplitudes are factored out of the integral by evaluating them in a frame where the struck nucleon's momentum has a constant "optimal" value. Such an approximation is clearly required in order to

derive a formula with the factorized structure of Eq. (5). The question of how best to choose this frame has been answered in the nonrelativistic theory by Gurvitz and collaborators.[4] The result depends on both momentum transfer and excitation energy. In the case of elastic scattering ($\omega=0$) the best choice is the Breit frame, in which the struck nucleon has momentum $\mathbf{p}=-\mathbf{q}/2$. At the quasielastic peak ($\omega=q^2/2m$), the struck nucleon is on average at rest, and the optimal frame is the two-body laboratory frame where $\mathbf{p}=0$. In the general case (arbitrary $\omega$), the struck nucleon's momentum is determined by requiring that it satisfies energy conservation:

$$\omega=(\mathbf{p}+\mathbf{q})^2/2m=p^2/2m \ ,$$

and that it lies along the only preferred direction: that of the momentum transfer $\mathbf{q}$. Then the optimal momentum is given by

$$\begin{aligned} \mathbf{p}_{\rm opt}&=-\frac{\mathbf{q}}{2}\left[1-\frac{2m\omega}{q^2}\right] \quad (nonrelativistic) \ , \\ \mathbf{p}_{\rm opt}&=-\frac{\mathbf{q}}{2}\left[1-\frac{\omega}{q}\left[1+\frac{4m^2}{q^2-\omega^2}\right]^{1/2}\right] \quad (relativistic) \ . \end{aligned} \tag{9}$$

The second line gives the result using relativistic kinematics. Note that $\mathbf{p}_{\rm opt}$ reduces to zero at the quasielastic peak and to the Breit-frame momentum at $\omega=0$.

Since the experimentally determined amplitudes are usually given in the center-of-mass (c.m.) frame, it is in general necessary to perform a Lorentz boost to the optimal frame. The method for performing this boost is described in Ref. 3. It involves extracting the invariant Dirac amplitudes from the c.m. amplitudes and then sandwiching them between Dirac spinors in the optimal frame. This boost is necessary for evaluating spin observables, but not for cross sections, since

$$\mathrm{tr}(f^{\dagger}_{\rm opt}f_{\rm opt})=\mathrm{tr}(f^{\dagger}_{\rm c.m.}f_{\rm c.m.})=\frac{d\sigma_{\rm NN}}{d\Omega_{\rm c.m.}} \ , \tag{10}$$

where the trace is over both projectile and target-nucleon spins. The c.m. cross section must, of course, be evaluated at the two-body energy determined from the optimal-frame kinematics.

Combinations of the $p-p$ and $p-n$ amplitudes appropriate for inclusive $(p,p')$ and $(p,n)$ reactions are given by

$$\begin{aligned} \frac{d\sigma_{\rm NN}}{d\Omega_{\rm c.m.}}&\rightarrow\frac{Z}{A}|f_{pp}|^2+\frac{N}{A}|f_{pn}|^2 \quad (p,p') \\ &\rightarrow\frac{N}{A}|f_{pp}-f_{pn}|^2 \quad (p,n) \ . \end{aligned} \tag{11}$$

$f_{pp}$ and $f_{pn}$ will be evaluated with their full angle and energy dependence using the Arndt phase-shift solutions.[13]

The most important aspect of the optimal frame is that the invariant two-body energy $s$ varies rapidly with $\omega$ due to its dependence on $\mathbf{p}_{\rm opt}$, and it can be quite different from the energy in the two-body laboratory frame. The effective laboratory kinetic energy at which the two-body amplitudes are evaluated in the optimal frame is given by

$$\begin{aligned} T_L^{\rm eff}&\equiv(s-4m^2)/2m \\ &=\frac{E_kE_{p_{\rm opt}}-\mathbf{k}\cdot\mathbf{p}_{\rm opt}-m^2}{m} \ , \end{aligned} \tag{12}$$

where $T_L$ denotes the kinetic energy, and $E_k=(k^2+m^2)^{1/2}$ is the full relativistic energy. $T_L^{\rm eff}$ can vary by several hundred MeV over the allowed region $-k_F<p_{\rm opt}<+k_F$, where $k_F$ is the Fermi momentum. Such variation will clearly have a large effect on the amplitudes in regions where they are strongly energy dependent.

To illustrate this point, and to show how well the optimal factorization works, we show in Fig. 3 calculations of the 164-MeV $^{58}$Ni$(p,p')$ cross sections as a function of the outgoing kinetic energy $T_L'$ at various scattering angles using a relativistic Fermi-gas model of the nucleus [see Eq. (13) below]. Solid curves show the "full" results with no factorization, in which the NN amplitudes are included inside the integral over the struck nucleon's momentum, and the dashed curves in the upper figure show the corresponding results based on the optimal factorization (Eq. 5). In the lower figure the amplitudes have been evaluated in the two-body lab frame where the struck nucleon is assumed to be at rest—an approximation often used in inelastic scattering calculations. We see that the optimal factorization provides an excellent approximation to the full integration, whereas the two-body lab factorization does poorly, especially at the larger angles. At very large angles (in this case above 80°) the two-body lab frame is not even well defined, because the quasielastic point $\omega=(q^2+m^2)^{1/2}-m$, which determines the lab frame, moves below $\omega=0$. The problem is that a nucleon at rest cannot contribute to the cross sec-

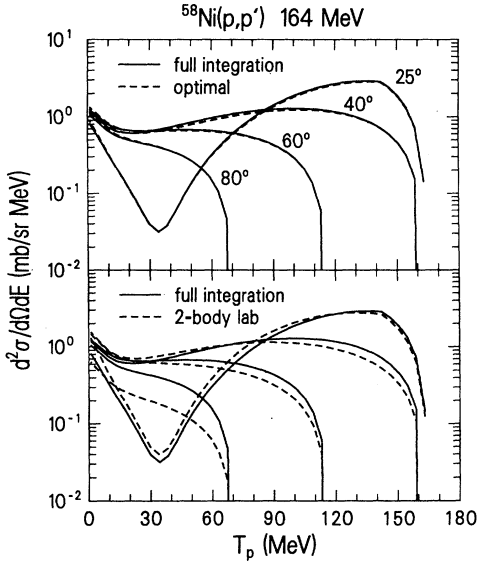


FIG. 3. $(p,p')$ cross sections based on Eq. (5) with optimal and two-body lab factorization of the NN amplitudes. In the solid curves the amplitudes are inside the integration over the struck nucleon's Fermi momentum.

tion at arbitrary angles and energy transfers without violating energy conservation at the two-body level. The optimal factorization, on the other hand, was constructed to satisfy energy conservation, and provides a simple yet accurate means of including the effects of Fermi motion.

### C. Distorted-wave Fermi-gas model

At the large energy losses with which we are concerned, the cross sections are not sensitive to finite-nucleus effects such as discrete states and giant resonances. Therefore, a Fermi-gas model of the nucleus should be adequate. The nuclear response function which enters into Eq. (5) is given in the relativistic Fermi-gas model by

$$R(q,\omega)=\frac{3}{4\pi k_F^3}\int d^3p\,\Theta(k_F-p)\Theta(|\mathbf{p}+\mathbf{q}|-k_F)\times\delta(\omega-E_{\mathbf{p}+\mathbf{q}}+E_p)$$
$$=\frac{3}{2k_F^3}\left[\frac{\omega}{2q}(k_F^2-k_L^2)+\frac{1}{3q}(E_{k_F}^{3/2}-E_{k_L}^{3/2})\right], \tag{13}$$
$$k_L=\left[\frac{|\mathbf{p}_{\rm opt}|}{[(E_{k_F}-\omega)^2-m^2]^{1/2}}\right]_> .$$

$R(q,\omega)$ should be set to zero if the above expression is negative. In the last line $k_L$ is the greater of the two quantities in large square brackets, and the relativistic version of $\mathbf{p}_{\rm opt}$ in Eq. (9) should be used. Following Ref. 14, the effect of the nuclear potential well is taken into account approximately by measuring both projectile and target-nucleon energies from the bottom of the Fermi sea in the evaluation of the response function and the NN amplitudes (but not in the evaluation of $\sigma_{\rm NN}$ and $N_{\rm eff}$, since the empirical optical potential was given as a function of the laboratory kinetic energy).

Equation (13) gives the response of the Fermi-gas to a plane-wave probing field. The effects of distortion can be included in a relatively simple model based on the distorted-wave impulse approximation and the eikonal approximation. In Ref. 3 such a model was presented in which the probing field included the full spin-dependent eikonal distorted waves as well as the optimal-frame amplitudes. The full response in this model is expressed in terms of a convolution integral of the plane-wave response with a distortion function and the NN amplitudes:

$$S(q,\omega)=\int\frac{d^2q'_\perp}{(2\pi)^2}R(\mathbf{q}-\mathbf{q}'_\perp,\omega)|\Delta(\mathbf{q}'_\perp)f_{\rm opt}(\mathbf{q}-\mathbf{q}'_\perp)|^2 ,$$
$$\Delta(\mathbf{q}'_\perp)=\int d^2b\,\exp(i\mathbf{q}'_\perp\mathbf{b})\exp[iS(\mathbf{b})]T^{1/2}(b) , \tag{14}$$

where $\mathbf{q}'_\perp$ is the momentum transferred in the distortion. A factor $C^{1/2}$ (c.f. Eq. 5) has been absorbed into the definition of $f_{\rm opt}$ to simplify the formula. $T(b)$ is the "thickness function," which is the integral of the density along the projectile's trajectory at impact parameter $b$, and $S(\mathbf{b})$ is the eikonal phase, which is the integral of the optical potential along the same trajectory. Equation (14) is slightly more complicated if spin-dependent distortion is included, in which case $\Delta$ becomes a matrix and $f_{\rm opt}$ a vector in the space of projectile spin matrices. However, the most important term contributing to the eikonal phase is the imaginary central optical potential, which confines the scattering to the nuclear surface, and for our purposes it is sufficient to retain only this term. Then, in the limit of a short-range NN interaction, the eikonal phase reduces to the simpler form $iS(\mathbf{b})\rightarrow\sigma T(b)/2$, where $\sigma$ is again the in-medium NN cross section given by Eq. (7), and the distortion function satisfies

$$\int\frac{d^2q'_\perp}{(2\pi)^2}|\Delta(\mathbf{q}'_\perp)|^2=N_{\rm eff}(0,0) . \tag{15}$$

Thus, except for the angle and energy dependence of $N_{\rm eff}$, Eq. (5) can be recovered from Eq. (14) by factoring $f_{\rm opt}$ and $R(q,\omega)$ out of the integral and evaluating them at the external momentum transfer $\mathbf{q}$. As we will see, the dominant effect of the distortion integral is at forward angles, so the angle and energy dependence of the final-state absorption can be approximately included in Eq. (14) by simply renormalizing the cross section as follows:

$$\frac{d^2\sigma}{d\Omega\,d\varepsilon}=N_{\rm eff}(\theta,\omega)S(q,\omega)/N_{\rm eff}(0,0) . \tag{16}$$

Figure 4 shows a sample calculation of the $^{27}$Al$(p,n)$ reaction at 113 MeV. Dashed curves are based on Eq. (5) using the plane-wave response function in Eq. (13), and the solid curves are the results of the distorted-wave model based on Eqs. (16), (14), and (13). We see that the effect of the distortion is to smooth out the cross sections as a function of $\omega=T_L-T'_L$. The largest effect is at forward angles where the convolution integral produces a long tail at low emission energy which is not present in the plane-wave calculation. At large angles it also produces a tail at the high-energy end of the spectrum. In these calculations we have chosen to evaluate the plane-wave response $R(q,\omega)$ at one-half nuclear matter density ($\rho_0=0.08$ fm$^{-3}$, $k_F=1.06$ fm$^{-1}$). A value of one-third

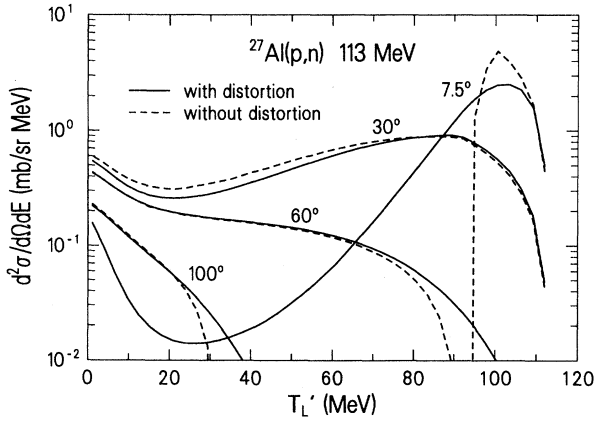


FIG. 4. Effect of momentum transfer in the distortion on quasielastic cross sections. Dashed lines are based on Eq. (5) and solid lines on Eqs. (14) and (16).

nuclear matter density was suggested in Ref. 15 from comparisons of slab-model and Fermi-gas surface response functions. We find that the value one-half yields slightly better agreement with the measured angle-dependent spectra in the 60–200 MeV region we are investigating, although the calculated results are not extremely sensitive to this choice.

The distorted-wave Fermi-gas model can also be extended to include random-phase approximation (RPA) correlations using an interacting Fermi-gas, as discussed in Ref. 3. We will return to this point later in the discussion of $(p,n)$ reactions, where a repulsive interaction in the isovector channels can dramatically alter the response.

## IV. COMBINING QFS WITH THE EXCITON MODEL

We have argued that the exciton model cannot accurately describe single-step processes, but it should nevertheless provide a reasonable description of multistep processes, since the total energy is shared among many particles and holes and the cross sections vary slowly with angle and energy transfer. While it is possible to evaluate multistep quasifree scattering using the same physical models as the single-step processes, such methods are numerically very complicated. Instead, we use the exciton model to describe these processes, with the aim of developing a relatively simple model. Eventually this assumption will have to be tested with more sophisticated calculations, but it should be emphasized that the most crucial ingredient in any model is an accurate description of the single-step processes, which, as we will see, constitute most of the reaction cross section.

To combine the quasifree scattering model presented in the last section with the exciton model, we insert it in place of the 2p1h term in Eq. (1):

$$\frac{d^2\sigma}{d\Omega\, d\varepsilon}=\frac{d^2\sigma_{\rm qe}}{d\Omega\, d\varepsilon}+\sigma_R\sum_{n=3{\rm p}2{\rm h},\ldots}\frac{D_n Q(n,\Omega)}{\Lambda_+^{(n)}+\Lambda_c^{(n)}}\rho_n(E,\varepsilon)\lambda_c(\varepsilon)\ . \tag{17}$$

The first term is the quasielastic cross section given by Eq. (5) or (16). In order that the integrated cross section adds up to the reaction cross section, the depletion factors $D_n$ must be modified. $D_n$ is the probability of making it to the $n$th stage of the reaction without emitting a particle, and is given by

$$D_n=\prod_{m=1}^{n-1}P_m\ ,\qquad P_m=\frac{\Lambda_+^{(m)}}{\Lambda_+^{(m)}+\Lambda_c^{(m)}}\quad (m>1)\ , \tag{18}$$

where $P_m$ is the probability of not emitting a particle in the $m$th stage. Therefore, $P_1$, the probability of not escaping after the first collision, is given by

TABLE I. Total reaction and quasielastic cross sections

| Target | $E$ (MeV) | $\sigma_R$ (mb) | $\sigma_{\rm qe}$ (mb) | %QFS |
|---|---|---|---|---|
| $^{54}$Fe | 62 | 836 | 516 | 62 |
| $^{58}$Ni | 164 | 774 | 539 | 70 |
| $^{27}$Al | 200 | 400 | 330 | 82 |
| $^{27}$Al | 113 | 431 | 333 | 77 |
| $^{27}$Al | 90 | 464 | 328 | 71 |
| $^{58}$Ni | 90 | 812 | 512 | 63 |
| $^{90}$Zr | 90 | 1214 | 633 | 52 |
| $^{209}$Bi | 90 | 1947 | 881 | 45 |

$$P_1=D_{3{\rm p}2{\rm h}}=1-\frac{\sigma_{\rm qe}(p,p')}{\sigma_R}\ . \tag{19}$$

$\sigma_{\rm qe}(p,p')$ is the integrated quasielastic $(p,p')$ cross section, which should be used to evaluate $P_1$ for both $(p,p')$ and $(p,n)$ reactions. The reason for this is that $\sigma_{\rm qe}(p,p')$ is the total quasielastic cross section, because it counts all collisions of the projectile with both target neutrons and protons. If one were to add $\sigma_{\rm qe}(p,n)$ to $\sigma_{\rm qe}(p,p')$ in Eq. (19), this would double the projectile-neutron collisions.

Table I shows the total reaction and quasielastic cross sections for all the nuclei and incident energies studied in this paper. The total quasielastic cross sections $\sigma_{\rm qe}=\sigma_{\rm qe}(p,p')$ were calculated by integrating Eq. (5) over scattering angles and emission energies [this is much simpler than integrating Eq. (16), and yields essentially the same results]. The reaction cross sections $\sigma_R$ were obtained from optical-model analyses.[16] We see that in all cases the single-step quasifree scattering dominates the reaction cross section. In the 90-MeV cases, the percentage of quasifree scattering ranges from 70% in $^{27}$Al to 45% in $^{209}$Bi. This behavior is what we would expect from simple geometric considerations: Quasifree scattering takes place in the nuclear surface region, which in lighter nuclei constitutes a larger percentage of the total cross-sectional area seen by the projectile. In heavier nuclei it is more likely that the projectile will penetrate into the interior, leading to multistep reactions. Roughly speaking, $\sigma_R$ increases as the cross sectional area (proportional to $A^{2/3}$, and $\sigma_{\rm qe}$ increases as the nuclear circumference (proportional to $A^{1/3}$).

## V. RESULTS AND DISCUSSION

In Fig. 5 calculated spectra are shown for the $^{54}$Fe$(p,p')$ reaction at 62 MeV. The solid lines are the full calculation based on Eq. (17), the long-dashed lines are the quasielastic contributions based on the distorted-wave model of Eqs. (14) and (16), and the remaining curves show the exciton contributions from 3p2h to 6p5h. Contributions from successive terms converge quickly. In this case, terms beyond 5p4h contribute only $\sim$2% of the total cross section. At the forward angles the quasifree contribution dominates the cross section, but the exciton contribution becomes comparable around 100° and dominates at backward angles. Solid dots in Fig. 5 show data from Ref. 17, and we see that in this case the calculations agree rather well with experiment,

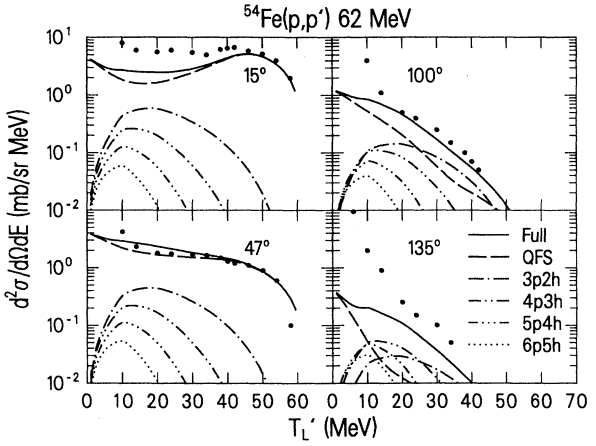


FIG. 5. QFS and exciton contributions to the full cross sections based on Eq. (17). Data are from Ref. 17.

especially at the intermediate angles which constitute most of the total cross section. At very low emission energies ( $< 10$ MeV) the calculations underpredict the data because we have not included the contribution from compound nucleus decay.

Figure 6 shows calculations of $(p,p')$ reactions for three nuclei at incident energies ranging from 62–200 MeV. Data for the $^{54}$Fe, $^{58}$Ni, and $^{27}$Al cases are from Refs. 17, 18, and 19, respectively. The plots on the left side show the results of pure exciton calculations based on Eq. (1), which has no phenomenological input. The pure exciton model gives a poor description of both angular and energy distributions. The shapes of the energy spectra are particularly bad in the 164 and 200 MeV cases, which reflects the inability of the exciton model to properly describe the first stage of the reaction at high incident energies. The plots on the right show the results of the QFS+exciton calculation based on Eqs. (17), (16), and (14). We see that the quasifree model does a much better job of describing the energy and angular distributions. At the intermediate angles ( $\sim 40°$ to 90°), which constitute the bulk of the total preequilibrium cross section, the agreement with the data is particularly good, and as a consequence we also find good agreement with angle-integrated cross sections (see Fig. 8). At the largest angles the exciton contribution dominates, and, as in the pure exciton case, the energy distributions are not as well described. We think this is primarily due to a failure of the angular dependence predicted by the free scattering kernel, which is proportional to the laboratory NN cross section derived from an isotropic c.m. cross section. The angular dependence of the two-body collisions is determined not only by the NN cross section, but also by the nuclear response function [see Eq. (5)], which unavoidably depends on both angle and energy loss. Furthermore, at high incident energies the NN cross sections are not isotropic, and even at low incident energies the effective two-body energy [Eq. (12)], which accounts for nuclear Fermi motion, can be very high. So it seems that the free scattering kernel should take into account not only the angular dependence of the two-body collisions, but also their dependence on incident energy and energy loss. Some work along these lines has already been done. In Refs. 20 the nuclear response function was included in the evaluation of the free scattering kernel, and this yielded larger contributions at backward angles. However, all these calculations follow Ref. 14 and employ a two-body lab NN cross section derived from an isotropic, and usually energy-independent, c.m. cross section. As we have discussed, at backward angles there is no contribution from collisions with nucleons at rest, and using two-body lab kinematics violates energy conservation. We suggest that it should be possible to improve the description of the angular dependence by employing the optimal-frame NN cross sections in the evaluation of the free scattering kernel.

At the most forward angles in Fig. 6, the QFS+exciton model does reasonably well at predicting the magnitude of the cross sections in the region of the quasielastic peak. However, at low and intermediate emission energies the forward-angle calculations underpredict the cross sections. This appears to be a general feature of our results which we do not yet completely understand. It is evidently not an effect of distortion, since this has been included in the calculations. The distortion does give a low emission tail to the quasielastic peak at forward angles (see Fig. 4), but it is not enough to explain the data. One possible explanation is that the two-step processes are much more forward-peaked than the 3p2h exciton term predicts. This speculation can only be answered by a full calculation of two-step quasifree scattering process. However, the two-step cross sections are expected to be much more isotropic than the single-step, and it seems unlikely that a full calculation will show a large enough angular variation to account for this feature. A more interesting possibility is that it is due to nuclear structure effects such as RPA p-h correlations or collisional damping of the nuclear response,[12] both of which can redistribute strength to lower emission energies. In continuum scattering, these effects are most important in channels involving spin and isospin transfer,[3] so they should be more pronounced in $(p,n)$ than in $(p,p')$ reactions. However, there is growing evidence that the $(p,p')$ continuum is predominantly spin response,[21] so the effects could show up there as well. We have performed some preliminary calculations which include these effects based on the methods described in Refs. 3 and 12, but they do not appear to be able to account for all of the excess strength. The collisional damping conserves the integrated strength, and can only increase the forward-angle cross section at intermediate emission energies by about a factor of 2, but in some cases (e.g., the 200-MeV, $^{27}$Al, 14° data) an increase of an order of magnitude or more is needed.

RPA correlations due to a strong repulsive residual p-h interaction in the isovector channels can have a dramatic effect on charge-exchange reactions. This can be seen in Fig. 7, which shows calculations of the 113-MeV $^{27}$Al$(p,n)$ cross sections at 7.5°, 30°, and 60°, along with data from Ref. 22. The upper two plots show the pure exciton and QFS+exciton calculations performed in the same way as those in Fig. 6. Again we see that the pure

exciton calculations fail badly to describe the data. The QFS+exciton results give considerable improvement, but at the two smaller angles the peaks of the calculated spectra occur at too high an energy. In the lower plot, the effect of RPA correlations is estimated by calculating the nuclear response function using the interacting Fermi-gas model described in Ref. 3. A repulsive residual interaction of 220 MeV fm$^3$ was used in both the spin and nonspin isovector response functions. This improves the shape of the calculated spectra, although the overall nor-

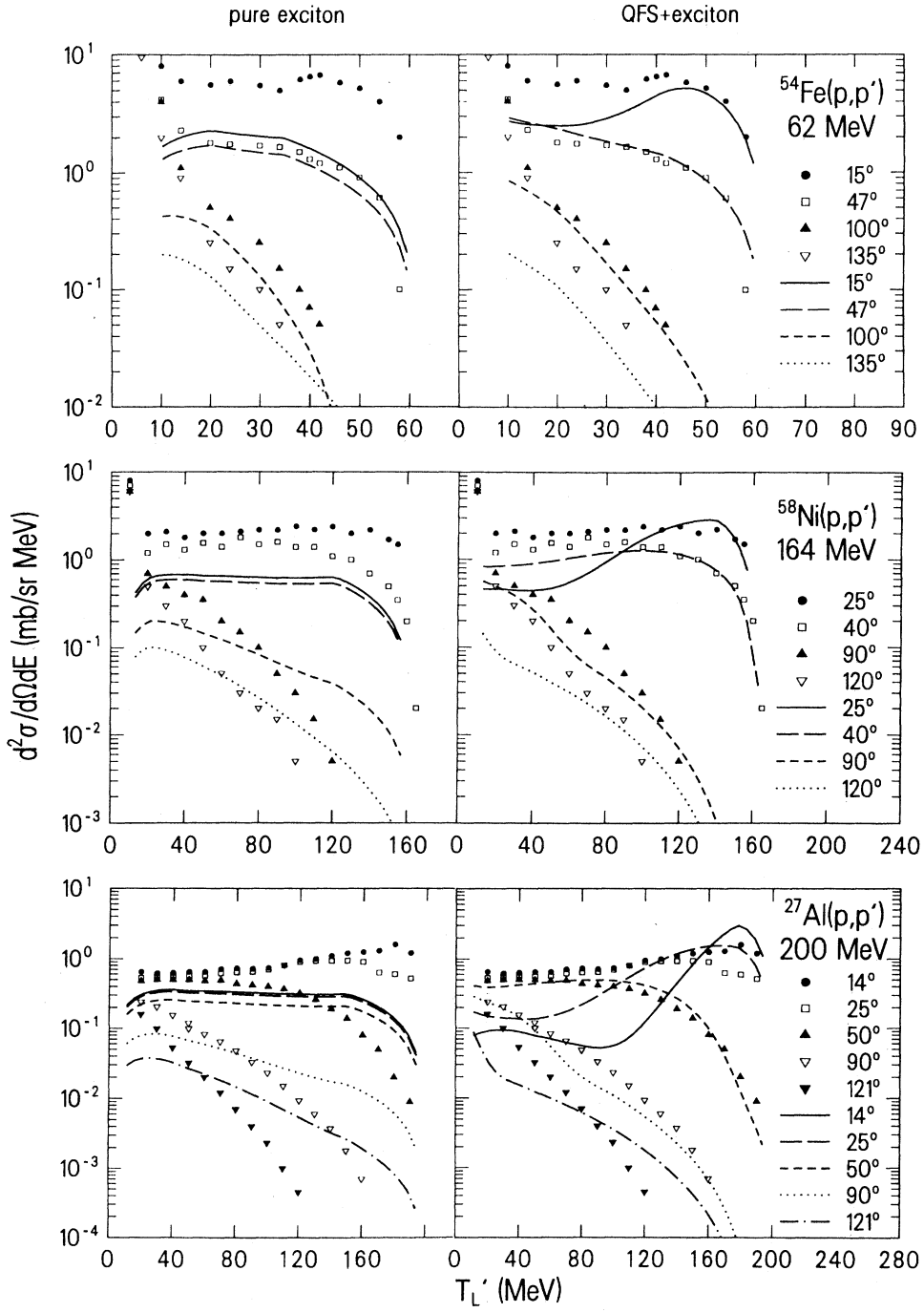


FIG. 6. Calculated ($p$,$p'$) spectra in the pure exciton and QFS+exciton models. Data for $^{54}$Fe, $^{58}$Ni, and $^{27}$Al are from Refs. 17, 18, and 19, respectively.

malization is somewhat low (a purely repulsive interaction will always reduce the integrated strength, since the RPA conserves the energy-weighted sum rule). At 7.5° the position of the quasielastic peak is shifted to lower emission energy by the RPA, but it is not enough to agree with the position of the peak in the data. We should emphasize that this calculation is a poor man's RPA: It does not include effects, such as the $q$ and $\omega$ dependence of the residual interaction, which may be important at large angles and energy transfers. Nevertheless, it does indicate that preequilibrium spectra can be sensitive to these correlations. Ultimately they may provide new experimental information which will constrain the behavior of the residual interaction at large $q$ and $\omega$.

Finally, in Fig. 8 we show calculations of angle-integrated $(p,p')$ and $(p,n)$ spectra for a variety of nuclei at 90 MeV, along with data from Ref. 23. To same computing time, the QFS terms were integrated using Eq. (5) rather than Eqs. (14) and (16). As with the total quasifree cross sections, it makes little difference if the effects of distortion are included in calculating the angle-integrated spectra. The results are in good agreement with the data for all cases considered, and the difference in the magnitude of the $(p,p')$ and $(p,n)$ cross sections is reasonably predicted. We emphasize again that there are *no free parameters* in these calculations. Furthermore, uncertainties in the angular dependence of the exciton terms do not effect the angle-integrated results. The high-energy end of the spectrum is almost entirely QFS, and the low-energy end is mostly the exciton contribution. Note that in the $^{209}$Bi case, where the fraction of exciton vs QFS is largest (see Table I), the $(p,p')$ cross section drops below the $(p,n)$ at the lowest emission energies. In the calculatin, this is due to the fact that the inverse cross section for protons (Eq. 3) vanishes at low energy due to the large Coulomb repulsion in bismuth. The physical interpretation in the actual $(p,p')$ reaction is that the escaping protons are accelerated by the Coulomb potential, and consequently appear at higher emission energies.

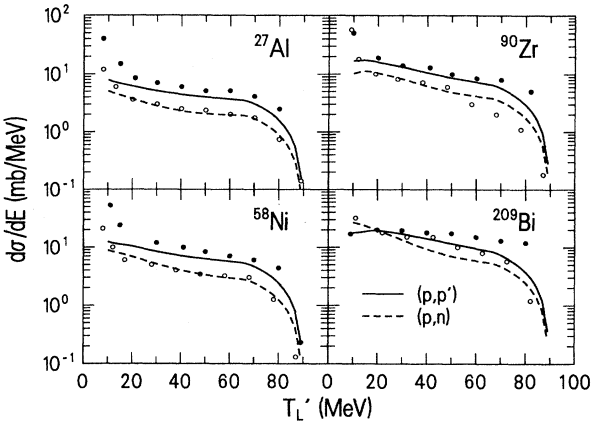


FIG. 8. Angle-integrated $(p,p')$ and $(p,n)$ spectra at 90 MeV along with data from Ref. 23.

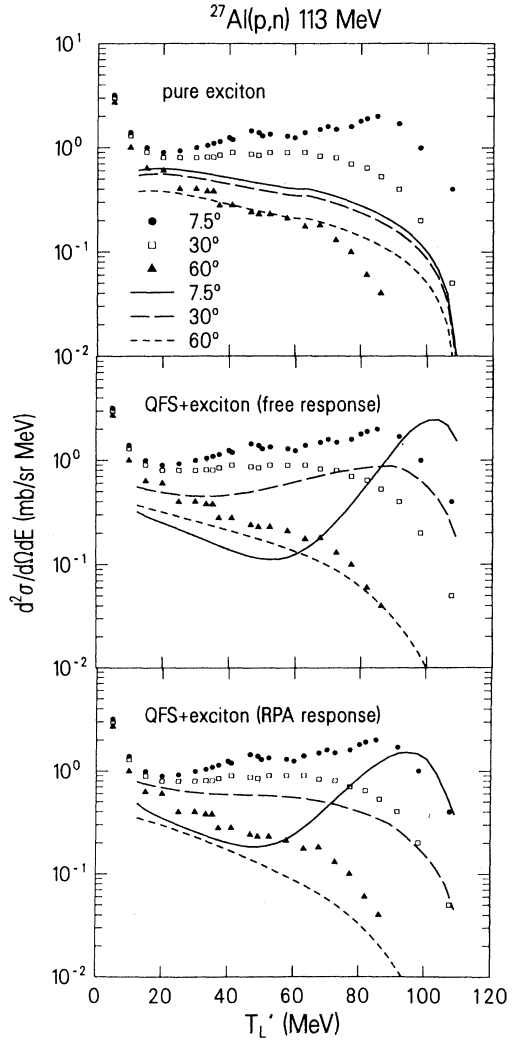


FIG. 7. $(p,n)$ cross sections with and without RPA correlations. Data are from Ref. 22.

## VI. CONCLUSION

We have presented a model of preequilibrium reactions based on single-step quasifree scattering and the exciton model for multistep contributions. The quasifree term dominates and provides a parameter-free description of the bulk of the angle-dependent energy spectra. We find major discrepancies only at very forward and backward angles. The latter can probably be remedied with an improved description of the angular dependence of the exciton terms. The forward-angle enhancement seen in the data at intermediate emission energies is not explained in the model, and may be associated with nuclear structure effects, or with multistep processes which are usually forward peaked.

In the energy region we have considered, the total quasielastic cross section constitutes 50% to 80% of the re-

action cross section. Therefore, the preequilibrium region consists primarily of direct single-step reactions. This is true even at quite large angles ( $< 100°$) where there is no pronounced quasifree peak. As a result, the preequilibrium region can be sensitive to nuclear structure effects usually only associated with low-lying discrete states and resonances, such as RPA correlations. This could provide a fertile ground for new research. In particular, measurements of spin observables in this region may make it possible to decompose the spin-isospin structure of the nuclear response at large excitation energy.

## ACKNOWLEDGMENTS

We would like to thank E. D. Arthur for useful comments and discussions and G. Reffo for collaboration in the initial stages of this study. This work was supported by the U.S. Department of Energy and the U.S. Air Force.

[1]H. Gruppelaar, P. Nagel, and P. E. Hodgson, Riv. Nuovo Cimento 9, 1 (1986).
[2]H. C. Chiang and J. Hüfner, Nucl. Phys. **A349**, 466 (1980).
[3]R. D. Smith, in *Proceedings of the International Conference on Spin Observables of Nuclear Probes, Telluride, Colorado, 1988* (Plenum, New York, in press).
[4]S. A. Gurvitz, Phys. Rev. C **33**, 422 (1986).
[5]J. Bisplinghoff, Phys. Rev. C **33**, 1569 (1986).
[6]F. C. Williams, Nucl. Phys. **A166**, 231 (1971); E. Běták and J. Dobeš, Z. Phys. **A279**, 319 (1976).
[7]J. M. Akkermans, H. Gruppelaar, and G. Reffo, Phys. Rev. C **22**, 73 (1980).
[8]J. W. Negele and K. Yazaki, Phys. Rev. Lett. **47**, 71 (1981); S. Fantoni, B. L. Friman, and V. R. Pandharipande, Phys. Lett. **104B**, 89 (1981).
[9]M. Blann and H. K. Vonach, Phys. Rev. C **28**, 1475 (1983).
[10]R. D. Smith and J. Wambach, Phys. Rev. C **36**, 2704 (1987).
[11]P. Schwandt, in *The Interaction Between Medium Energy Nucleons in Nuclei (Indiana Cyclotron Facility, Bloomington, Indiana)*, AIP Conf. Proc. No. 97, edited by Hans-Otto Meyer (AIP, New York, 1982).
[12]R. D. Smith and J. Wambach, Phys. Rev. C **38**, 100 (1988).
[13]R. A. Arndt *et al.*, Phys. Rev. D **28**, 97 (1983).
[14]K. Kikuchi and M. Kawai, Nuclear Matter and Nuclear Reactions (North-Holland, Amsterdam, 1968).
[15]H. Esbensen and G. F. Bertsch, Ann. Phys. **157**, 255 (1984).
[16]D. G. Madland, Proceedings of Specialists' Meeting on Preequilibrium Nuclear Reactions, Semmering, Austria, 1988, NEANDC-245'U'; P. Schwandt *et al.*, Phys. Rev. C **26**, 55 (1982).
[17]F. E. Bertrand and R. W. Peele, Phys. Rev. C **8**, 1045 (1973).
[18]R. E. Segal *et al.*, Phys. Rev. C **26**, 2424 (1982).
[19]H. Machner *et al.*, Phys. Lett. **138B**, 39 (1984).
[20]S. Ziyang, W. Shunuan, Z. Jinshang, and Z. Yizhong, Z. Phys. **A305**, 61 (1982); C. Costa, H. Gruppelaar and J. M. Akkermans, Phys. Rev. C **28**, 587 (1983); A. Iwamoto and K. Harada, Nucl. Phys. **A419**, 472 (1984).
[21]C. Glashausser *et al.*, Phys. Rev. Lett. **58**, 2404 (1987).
[22]M. M. Meyer (private communication).
[23]J. R. Wu, C. C. Chang, and H. D. Holmgren, Phys. Rev. C **19**, 659 (1979); A. M. Kalend *et al.*, *ibid.* **28**, 105 (1983).